BIOMOLECULES & THERAPEUTICS

Original Article
Biomol Ther 27(6), 540-552 (2019)

Alyssin and Iberin in Cruciferous Vegetables Exert Anticancer Activity in HepG2 by Increasing Intracellular Reactive Oxygen Species and Tubulin Depolymerization

Piman Pocasap[1], Natthida Weerapreeyakul[2,3,*] and Kanjana Thumanu[4]

[1]Research and Development in Pharmaceuticals Program, Graduate School, Faculty of Pharmaceutical Sciences, Khon Kaen University, Khon Kaen 40002,
[2]Division of Pharmaceutical Chemistry, Faculty of Pharmaceutical Sciences, Khon Kaen University, Khon Kaen 40002,
[3]Human High Performance and Health Promotion Research Institute (HHP&HP), Khon Kaen University, Khon Kaen 40002,
[4]Synchrotron Light Research Institute (Public Organization), Nakhon Ratchasima 30000, Thailand

Abstract

To determine the chemopreventive potential of alyssin and iberin, the *in vitro* anticancer activities and molecular targets of isothiocyanates (ITCs) were measured and compared to sulforaphane in hepatocellular carcinoma cell HepG2. The SR-FTIR spectra observed a similar pattern vis-à-vis the biomolecular alteration amongst the ITCs-treated cells suggesting a similar mode of action. All of the ITCs in this study cause cancer cell death through both apoptosis and necrosis in concentration dependent manner (20-80 μM). We found no interactions of any of the ITCs studied with DNA. Notwithstanding, all of the ITCs studied increased intracellular reactive oxygen species (ROS) and suppressed tubulin polymerization, which led to cell-cycle arrest in the S and G_2/M phase. Alyssin possessed the most potent anticancer ability; possibly due to its ability to increase intracellular ROS rather than tubulin depolymerization. Nevertheless, the structural influence of alkyl chain length on anticancer capabilities of ITCs remains inconclusive. The results of this study indicate an optional, potent ITC (viz., alyssin) because of its underlying mechanisms against hepatic cancer. As a consequence, further selection and development of effective chemotherapeutic ITCs is recommended.

Key Words: Isothiocyanates, Iberin, Alyssin, Reactive oxygen species, Tubulin depolymerization, HepG2

INTRODUCTION

Consumption of cruciferous vegetables is correlated with a reduction in the incidence of several types of cancer. The active ingredients responsible for chemopreventive activity are characterized as a group of unique compounds containing the –N=C=S moiety, and are called isothiocyanates (ITC) according to the functional group. ITCs have been identified in several Brassica plants (e.g., broccoli, cabbage, and radish) in the form of glucosinolate. Myrosinase enzyme, activated by plant damage, catalyzes the conversion of glucosinolates to ITCs possessing higher biological activities (Angelino and Jeffery, 2014). ITCs have been investigated for both their preventive and therapeutic activities against cancer in several cell- and animal-based assays. The major chemopreventive roles of ITCs include the reduction of phase I and induction of phase II metabolism enzymes related to carcinogenic activation. The modulation of these enzymes inactivates carcinogens and reduces the incidence of carcinogenesis. ITCs were reported to suppress cancer cell progression via various activities; for example, (a) inhibition of cell proliferation, (b) induction of cell-cycle arrest, (c) anti-angiogenesis, and (d) anti-metastasis (Pocasap *et al*., 2013; Veeranki *et al*., 2015).

Despite several studies on the anticancer activities of ITCs, there remains insufficient data on many ITCs to support their use as nutraceuticals, so they are overlooked as potential adjunctive agents. In the current study, two dietary ITCs, including iberin and alyssin, were examined for their anticancer activity in comparison with the most studied ITC, sulforaphane. Iberin was found to induce the phase II metabolism enzyme HO1 and γGCS in the fibroblast cell NIH3T3 (Ernst *et al*., 2013), and TR1 in the human breast cancer cell MCF-7 (Wang *et al*., 2005), while alyssin inhibited the phase I metabolism enzyme

Open Access **https://doi.org/10.4062/biomolther.2019.027**

Received Feb 12, 2019 **Revised** May 19, 2019 **Accepted** Jun 17, 2019
Published Online Aug 13, 2019

***Corresponding Author**
E-mail: natthida@kku.ac.th
Tel: +66-43-202378, Fax: +66-43-202379

cytochrome p450 1A1 and 1A2 activity induced by the carcinogen in MCF-7 cells (Skupinska *et al*., 2009). Both iberin and alyssin could induce cancer cell death *in vitro*. Iberin caused caspase-cascade activation, leading to neuroblastoma cell death through apoptosis (Jadhav *et al*., 2007). The induction of cancer cell growth arrest and apoptosis by iberin was also evidenced in human colon carcinoma cell Caco-2 by modulation of phase II enzyme and histone protein (Jakubikova *et al*., 2006). Alyssin induced apoptosis in leukemic cells and displayed high selectivity to the cancer cell line against the respective normal cell line (Misiewicz *et al*., 2007). Notwithstanding, the underlying mechanisms or molecular targets related to the cell death inducing ability remain undefined.

ITCs can be absorbed through the gastro-intestinal tract. After oral absorption, the ITCs go through the hepatic portal veins to liver where the first-pass metabolism occurs. The metabolic process yields metabolites and reduces ITC concentrations before distribution to other body tissues (Traka, 2016). In this study, the hepatocellular carcinoma cell line HepG2 was thus used as a liver cancer model because high-concentration of ITCs could be achieved after oral administration before first-pass metabolism. The present study aimed to investigate the molecular components responsible for cell death induction of iberin and alyssin in HepG2 cells. Due to the electrophilicity of the ITC functional group, the molecules are susceptible to interact with intracellular nucleophiles (Tian *et al*., 2016). We examined three possible molecular targets—DNA, ROS, and tubulin—comprising intracellular nucleophiles that possibly interact with ITCs, and resulting in cell death. Cell-phase arrest was analyzed as a subsequent cellular event. The endpoint for anticancer activity measurement includes cell viability, apoptosis, and necrosis; these too were determined as results of the molecular interaction. Synchrotron radiation-based Fourier transform infrared spectroscopy (SR-FTIR) was used to detect global biomolecular changes in HepG2 cells after ITC treatment. Sulforaphane was tested in all experiments as an ITC standard. Our previous study reported the correlation between structural alteration at the ITC side chain (including oxidation state of sulfur atom, number of double bond, and number of aromatic ring) and anticancer activity (Pocasap *et al*., 2018). Since structural alteration on the chain length was also noticed between the studied ITCs (iberin (3C), sulforaphane (4C), and alyssin (5C)), the influences of chemical structure correlation on activity were also analyzed and discussed.

MATERIALS AND METHODS

Materials

Iberin (3-(methylsulfinyl)-propyl isothiocyanate) (>97% purity), alyssin (5-(methylsulfinyl)-pentyl isothiocyanate) (>97% purity), and anti-tubulin antibody-Alexa Fluor® 488 (ab195883) were purchased from Abcam (Cambridge, MA, USA). Sulforaphane (4-(methylsulfinyl)-butyl isothiocyanate) (>95% purity) was purchased from Calbiochem (EMD, Darmstadt, Germany). Propidium iodide (PI) was purchased from BioLegend (San Diego, CA, USA). Bovine serum albumin was purchased from Amresco (Solon, OH, USA). Triton-X was purchased from USB Corp (Cleveland, OH, USA). Glycine and Tris were purchased from Vivantis (Selangor Darul Ehsan, Malaysia). Highly-polymerized calf-thymus DNA, goat serum, RNase, 2′,7′-dichlorodihydrofluorescein diacetate (DCFH-DA), 4′-6-diamidino-2-phenyl indole (DAPI), 4-(4′-Nitrobenzyl)pyridine (NBP), and anticancer drug melphalan were purchased from Sigma-Aldrich Co (St. Louis, MO, USA). The reagents used in the cell-based assay were of molecular biological grade. Culture media (RPMI-1640), fetal bovine serum (FBS), penicillin/streptomycin, and 0.25% Trypsin-EDTA (1X) were bought from Gibco (Grand Island, NY, USA). All other chemicals and solvents were of reagent grade and used without purification. Stock solutions of the ITCs were freshly prepared prior to use by dissolving them in DMSO; the final DMSO concentrations were not to exceed 0.2% v/v so as to avoid any DMSO cytotoxic effect on the experimental results.

Cell lines and culture

The human hepatocellular carcinoma cell HepG2 (ATCC# HB-8065) and African green monkey kidney normal cell Vero (ATCC# CL-81) were purchased from the American Type Culture Collection (Manassas, VA, USA). RPMI-1540 was used as a culture media supplemented with 10% fetal bovine serum, and 1% Pen/Strep (100 unit/ml penicillin and 100 μg/ml streptomycin). The cells were incubated in a CO_2 incubator (95% air and 5% CO_2, 37°C) until they reached 70-80% confluence before use.

FTIR spectroscopy analysis

FTIR measurements were recorded at the infrared microspectroscopy beamline at the Synchrotron Light Research Institute (Nakhon Ratchasima, Thailand). Sample preparation was performed as previously described (Junhom *et al*., 2016). The samples—cells spotted on the BaF_2 window—were analyzed in the transmission mode using a Bruker Vertex 70 spectrometer connected to a Bruker Hyperion 2000 microscope (Bruker optic Inc, Ettlingen, Germany). The synchrotron light was used as the IR source for FTIR measurement. The FTIR spectrometer was equipped with a potassium bromide beam splitter and the microscope was coupled with a MCT (HgCdTe) detector cooled with liquid nitrogen, attached with a PIKE MIRacle (Madison, WI, USA). Sixty-four scans—ranging between 4,000 and 600 cm^{-1}, with 4 cm^{-1} spectral resolution—were recorded and averaged for each spectrum using OPUS 6.5 software (Bruker optic Inc).

Unscrambler® X software (version 10.1, CAMO Software AS, Oslo, Norway) was used to identify any significant variation between data sets in Principle Component Analysis (PCA) covering a spectral range of 3,000-2,800 cm^{-1} and 1,800-900 cm^{-1}. The primary spectra were smoothed using the Savitzky–Golay algorithm (with 13 points of smoothing; thereby minimizing the effects of variable baselines). The smoothed spectra were then normalized using extended multiplicative signal correction (EMSC). The process normalized spectra accounting for differences in sample thickness and correcting for scattering artifacts. Six principal components (PCs) were considered for classification and three PCs (PC1, PC2, and PC3) were chosen for analysis. 2D score plots were used to display the clustering of dataset, and correlation loading plots were plotted to determine the variation in the data set.

Unsupervised hierarchical cluster analysis (UHCA) using Ward's algorithm was applied to test for degree of similarity of the FTIR spectra. The analysis utilized a matrix to define inter-spectral distances for identification of the most similar spectra. The spectral distance between the remaining and

new clusters were then recalculated. UHCA was performed using OPUS 6.5 software (Bruker optic Inc) in the spectral range 3,000-2,800 cm^{-1} and 1,800-900 cm^{-1}. The FTIR spectral ranges were classified as (1) the lipid region: 3,000-2,800 cm^{-1}; (2) the protein region: 1,800-1,480 cm^{-1}; and, (3) the nucleic acid region: 1,280-900 cm^{-1} due to the components being presented mainly in the region (Machana *et al*., 2012; Baker *et al*., 2014). The integrated peak areas of FTIR spectra were determined using the OPUS 6.5 software (Bruker optic Inc) in (1) the lipid region: 3,000-2,800 cm^{-1}; (2) the protein region 1,800-1,480 cm^{-1}; and, (3) the nucleic acid region: 1,280-900 cm^{-1}. The amide I spectra (1,300-950 cm^{-1}) were analyzed for secondary protein structure by curve-fitting analysis (Gaussian and Laurence algorithm) on average spectra.

Cell viability assay

Cell viability was assessed using neutral red (NR) assay as previously described (Junhom *et al*., 2016). In brief, cells—at a density of 4×10^5 cells/ml (100 μl/well) in a 96-well plate—were incubated with ITCs at various concentrations (0.1-160 μM) for 24 h. The cells were then washed using PBS and incubated with NR (50 μg/ml) for 2 h at 37°C. Cells were washed again using PBS and solubilized with 0.33% v/v HCl in isopropanol. The absorbance was measured using a Sunrise™ microplate absorbance reader (Tecan Austria Gmbh, Grödig, Austria) at 520 nm (reference wavelength; 650 nm). The percentage of cell viability was calculated vis-à-vis the untreated cells and cytotoxicity was presented as the inhibition concentration at 50% (IC_{50}). DMSO was used (<0.2%v/v) and showed no cytotoxicity. Selectivity index (SI) was determined as the ratio of $IC_{50\ (Vero)}$ to $IC_{50\ (HepG2)}$ of each ITC.

Mode of cell death determination by Annexin V/PI staining

The mode of cell death was determined using Annexin V and propidium iodide (PI) staining according to the manufacturer's instructions (Bender MedSystem GmbH, Vienna, Austria). Briefly, the treated cells were harvested and re-suspended in binding buffer (1X) (BD Biosciences, San Jose, CA, USA). Annexin V and PI were then added and incubated at room temperature in the dark for 15 min. The stained cells were analyzed using a fluorescent-activated cell sorter (FACS)

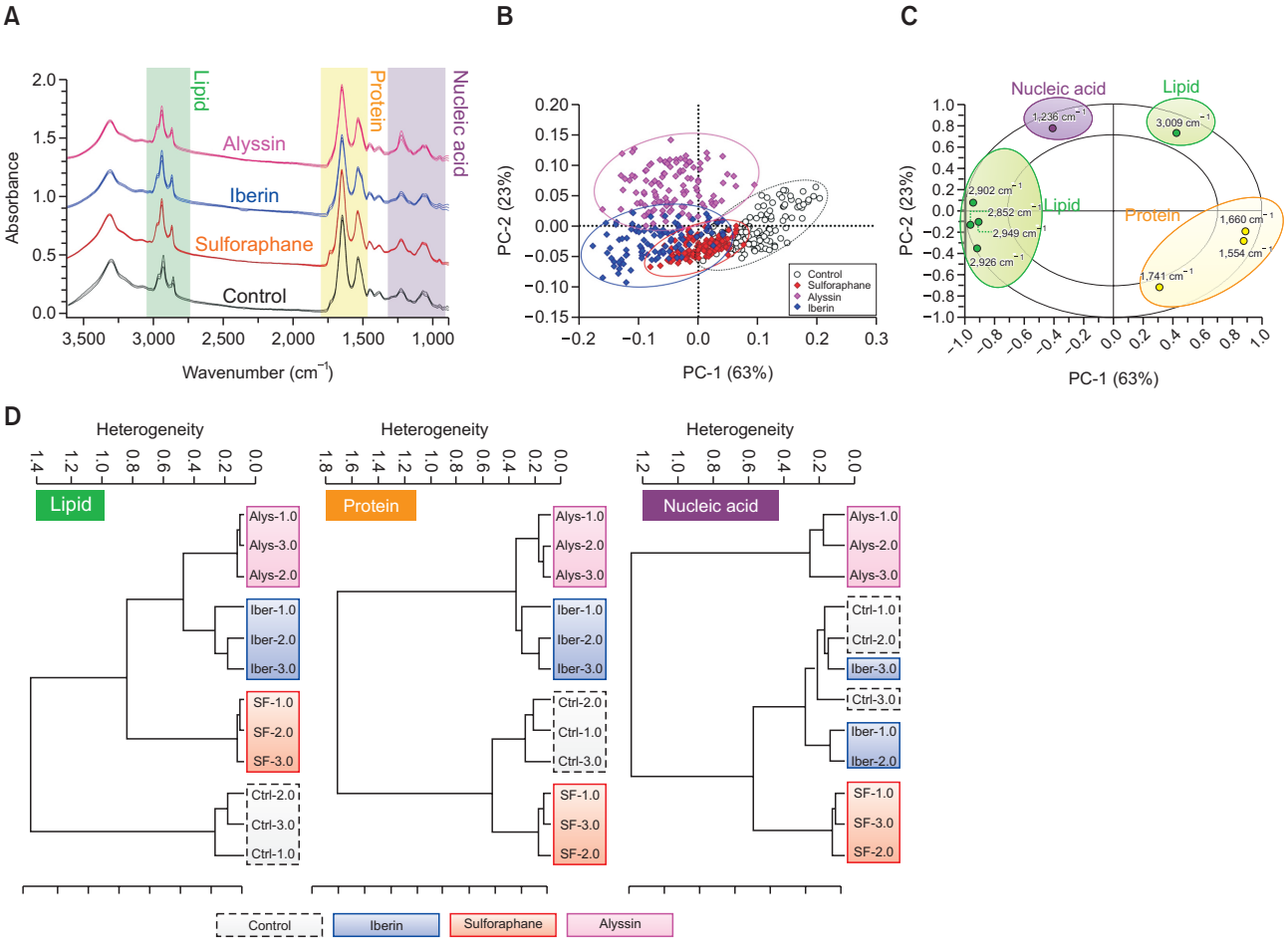

Fig. 1. FTIR spectral analysis of HepG2 treated with ITCs at 80 μM for 24 h. Mean spectra in each treatment group displayed as solid line and parallel line indicating standard deviation (A). PCA score plot on PC1 and PC2 indicate spectral clusters of respective treatment group (B). PCA correlation loading plot represents wavenumbers discriminating spectral differences among ITCs and control treatment (C). Hierarchical classification of spectra based on Ward's algorithm on lipid (3,000-2,800 cm^{-1}), protein (1,800-1,480 cm^{-1}), and nucleic acid (1,280-900 cm^{-1}) region (D).

analyzer (BD FACSCanto II, Franklin Lakes, NJ, USA).

Cell phase analysis and cell-based tubulin polymerization assay

Determination of cell phase and tubulin polymerization was performed as previously described (Pocasap *et al*., 2018). HepG2 cells were treated with 10, 20, and 40 μM ITCs for 12 h. The cells were collected and washed with cold 0.9% NaCl, then fixed with cold ethanol (80%, for 15 min). The fixed cells then were permeabilized (0.5% triton-X in PBS) and blocked against other nonspecific proteins (viz., 1% BSA (bovine serum albumin), 10% goat serum, 0.3 M glycine, in 0.1% tween, and 0.05% triton-X in PBS) for 30 min at 4°C. HepG2 cells then were incubated with tubulin antibody (2.5 μg/ml) at room temperature for 3 h, then RNase (120 μg/ml) and PI (20 μg/ml) were added for 30 min at room temperature. The FACS analyzer (BD FACSCanto II) was used to examine the stained cells. The proportion of G_0/G_1, S, and G_2/M was calculated using FCS Express 5 software (Glendale, CA, USA). The G_2/M cells were graded and used to determine tubulin level based on the geometric mean of tubulin intensity.

DNA alkylation by NBP assay

The alkylating activity of ITCs was determined by 4-(*p*-nitrobenzyl)pyridine (NBP) assay as previously described (Nonpunya *et al*., 2018). ITCs (1 mM) were incubated with NBP (20 mM) in NBP buffer solution (pH 4.0) at 70°C, from 0 to 40 min. The solutions were added to the mixture of ethanol and cold 0.1 N NaOH. The alkylated products yielded a blue-colored solution, which were then measured at 600 nm with the Sunrise™ microplate absorbance reader (Tecan Austria Gmbh).

DNA interaction by Circular dichroism (CD)

Interactions between the calf-thymus DNA and the ITCs were investigated as previously reported (Agarwal *et al*., 2013). Briefly, calf-thymus DNA at a constant 50 μM was incubated with cisplatin (positive control) or ITCs at various molar ratios (1:0.5 to 1:10) in Tris buffer pH 7.2, 37°C, for 3 h. Jasco-815 CD spectrometer (JASCO, Tokyo, Japan) was used to record CD spectra of calf-thymus in the reaction mixture in the far UV region (200-300 nm). An average of three scans (at a scan speed of 50 nm/min) was taken for all experiments.

Intracellular ROS level detection by DCFH-DA assay

Intracellular ROS levels were measure by 2′,7′-dichlorodihydrofluorescein diacetate (DCFH-DA), as previously reported (Pocasap *et al*., 2018). DCFH-DA is oxidized by intracellular ROS to 2′,7′-dichlorofluorescein (DCF)—a fluorescent compound detected by flow cytometer. HepG2 cells were treated with ITCs at different concentrations (10, 20, and 40 μM) for 12 h. Cells were then collected and incubated with DCFH-DA (10 μM) in the dark for 30 min at room temperature. The cells were subsequently washed with PBS and analyzed using the FACS analyzer (BD FACSCanto II). Intracellular ROS levels were calculated by BD FACSDiva software and expressed as a percentage of DCF intensity vis-à-vis the cell population in each treatment.

In vitro tubulin polymerization assay

To determine tubulin polymerization *in vitro*, a Tubulin Polymerization Assay kit (Cytoskeleton, Denver, CO, USA) was used as per the manufacturer's instructions. Briefly, a reaction mixture containing (1) tubulin, (2) GTP, (3) Buffer 1, and (4) Tubulin Glycerol Buffer were mixed and kept on ice. Then, the respective aliquot of 5 μl of ITC in deionized H_2O (final concentration 40 μM) was added in a 96-well plate, and warmed for 1 min at 37°C in an incubator. Tubulin polymerization was initiated by adding 50 μl of reaction mixture and monitored for fluorescent intensity (E_x=360 nm; E_m=420 nm). Measurement was recorded using a Varioska Flash spectral scanning multimode reader, Thermo Fisher Scientific (San Jose, CA, USA).

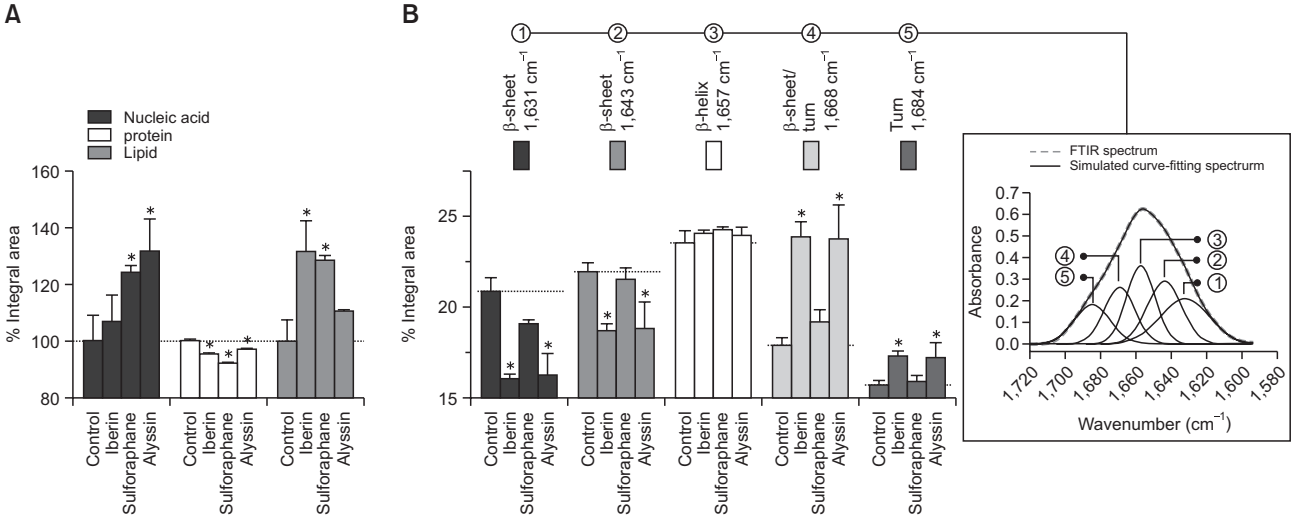

Fig. 2. Histogram represents mean integral area of respective lipid (3,000-2,800 cm^{-1}), protein (1,800-1,480 cm^{-1}), and nucleic acid (1,280-900 cm^{-1}) region in each treatment group (A). Integral area of secondary structure proteins corresponds to curve-fitting analysis. Inset graphic illustrates FTIR absorbance of amide I band contour with best-fit 50% Loentzian/Gaussian individual components band. RMS error <0.005 in all treatment groups (B). HepG2 treated with 80 μM ITCs for 24 h. All data presented as mean ± SD (n=3). *p<0.05, significant difference compared to control.

Readings were taken in the kinetic mode for 1 h (for a total of 61 readings).

Morphological changes of DNA and microtubule by fluorescent microscopy

DNA and microtubule morphological changes were examined using fluorescent microscopy as in a previous study (Pocasap *et al*., 2018). HepG2 cells were seeded into 96-well plates for 24 h prior to be treated with 40 μM ITCs for 12 h. The cells were then washed with cold 0.9% NaCl, then fixed with cold ethanol (80%, 15 min). The fixed cells were then permeabilized (0.5% triton-X in PBS) and blocked against other nonspecific proteins (1% BSA, 10% goat serum, 0.3 M glycine, in 0.1% tween and 0.05% triton-X in PBS) for 30 min at 4°C, respectively. HepG2 cells were then incubated with tubulin antibody (2.5 μg/ml) at room temperature for 3 h. The cells were subsequently washed with PBS and incubated with 0.3 μM DAPI at 4°C for 15 min. The stained cells were washed with PBS again and 100 μl of PBS was added to each well before being observed under microscope. A fluorescent microscope EVOS™ FL Auto 2 (Thermo Fisher Scientific) was used to analyze and record at 10X magnification. Micro Studio Image analysis software (Thermo Fisher Scientific) was used for the image processing and DAPI stain nuclei were visualized as magenta for higher contrast in the merged images.

Statistical analysis

The data were displayed as a mean ± SD. The results were analyzed prior to further statistical analysis for normality of distribution (Shapiro-Wilk test) and homogeneity of variance (Levene's test). A pass was indicated when *p*-values were >0.05. Differences among any treatments were defined using one-way ANOVA followed by a Tukey's multiple comparison post hoc test using SPSS 19.0 for Windows® (SPSS Inc., Chicago, IL, USA). Any differences with a *p*-value <0.05 were considered statistically significant.

RESULTS

FTIR

The primary FTIR spectra of HepG2 cells treated with ITCs (80 μM, 24 h) compared with the untreated (control) cells are displayed in Fig. 1A in spectral regions ranging from 3,500 to 900 cm^{-1}. The IR spectral regions can be categorized into 3 main regions according to major biological components presented in each region (Machana *et al*., 2012; Junhom *et al*., 2016). The lipid region (3,000-2,800 cm^{-1}) comprises the CH_2 and CH_3 bond vibration from the lipid acyl chains—the hydrophobic tail of phospholipid bilayer—forming cells and organelle membranes. The protein region (1,800-1,480 cm^{-1}) is assigned according to the vibration of the amide bond, which links amino acid units in protein chains, and displays two major peaks near 1,600 cm^{-1}—including the amide I (stretching vibration) and amide II (bending vibration) bands. The nucleic acid region (1,280-900 cm^{-1}) is distributed mainly from the vi-

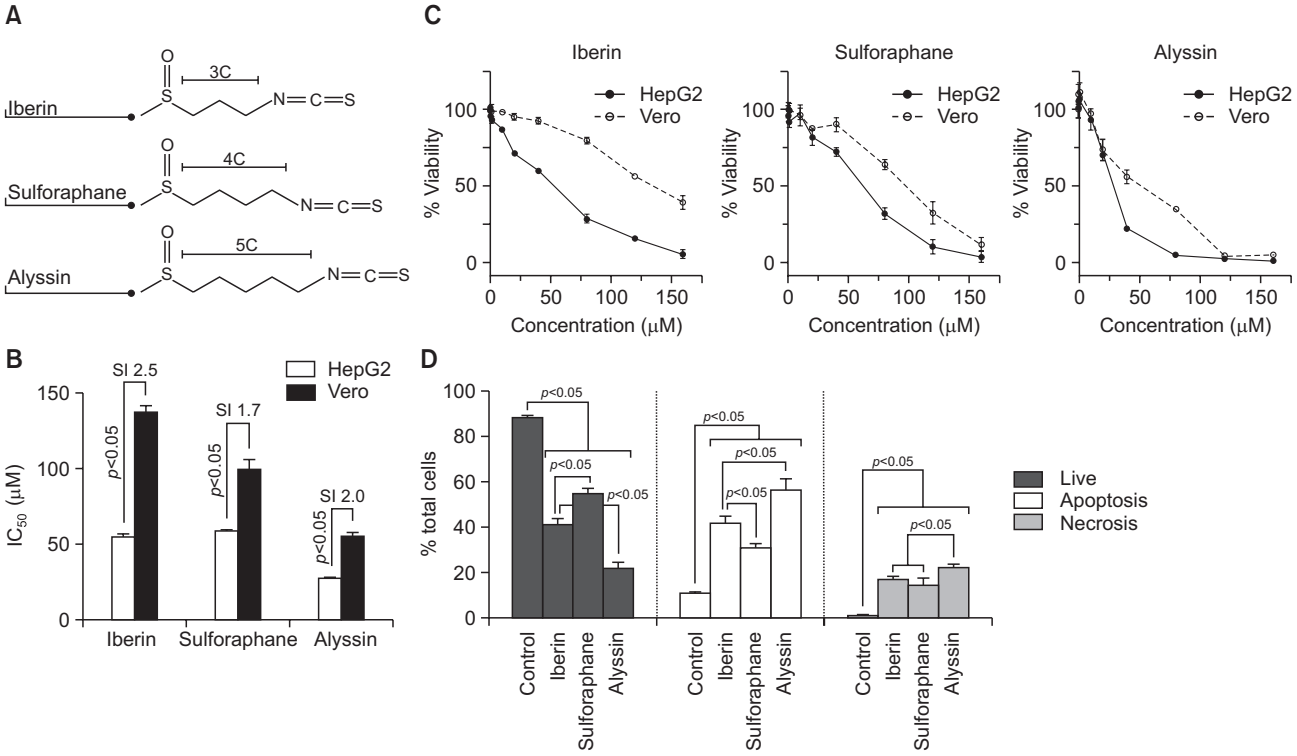

Fig. 3. Anticancer activity of ITCs on HepG2 cells after treatment for 24 h: structure (A), IC_{50} (B), cell viability profile (C), and mode of cell death (D). Cell viability presented as percentage relative to untreated control. In mode of cell death study, HepG2 cells treated with 80 μM ITCs. Living, apoptotic, and necrotic represented as percentage to total cell population in each treatment group. All data presented as mean ± SD (n=3).

bration of phosphodiester bond, making up the backbone of nucleic strand in DNA and RNA.

PCA analysis was applied to determine the data spreading and clustering as well as to indicate the contribution of variables (wavenumbers) that are different between the treated groups. Our PCA score plot shows that the IR spectra of the ITC treated groups—in contrast with the untreated group—were shifted to the left of PC1 (x-axis in Fig. 1B). PC1 explains 63% of the total variance among the treatment groups while PC2 (y-axis, Fig. 1B) explains the remaining 23%. The PCA correlation loading plot thus displays wavenumbers corresponding to the PCA score plot and indicates the causes of pattern variation. The wavenumbers—indicated in the radius between eclipses—are strongly responsible for the causes of variation, discriminating along the PC1 and PC2 axis. According to the number of wavenumbers presented in each region, the most discriminating wavenumbers were in the lipid (5 wavenumbers) and protein (3 wavenumbers) regions (Fig. 1C), indicating that the lipids and proteins were the most altered biological components after treatment with ITCs.

Hierarchical cluster analysis (HCA) was then used to describe the similarities and differences among the spectra from the four treatment groups—control, iberin, sulforaphane, and alyssin—by creating a dendrogram of the results. Based on Ward's algorithm, spectral analysis by HCA was conducted on three different regions including the lipids, proteins, and nucleic acids (Fig. 1D). In the lipid region, the ITC treated groups were clearly separated from the control group with a heterogeneity score of 1.4. In the protein region, the alyssin and iberin treated groups were different from the control group with a heterogeneity score of 1.6. In the nucleic acid region, only the alyssin treated group could be separated from the control—with a heterogeneity score of 1.2. The HCA result indicated that the spectral differences between the groups treated with ITCs and the control occur mainly in the lipid region where all ITC treated groups can be definitively separated from control. The rank of discriminating spectral regions was thus lipid, protein, and nucleic acid. The HCA result was in accordance with the PCA, indicating that lipids and proteins are the major discriminating IR spectral regions when comparing between ITC treatment and control. In conclusion, lipids and proteins were mainly altered after ITC treatment in HepG2 cells.

The integral area histogram of each biological component region was illustrated as a percentage of the control (100%) (Fig. 2A). All groups treated with ITCs displayed a similar pattern of biological component alteration, including an increase in nucleic acid (106.6-131.4%) and lipid components (110.5-131.4%), and a subtle decrease in proteins (96.9-91.9%). A curve-fitting procedure was used to study proteins by discerning the absorption bands of the spectral interval corresponding to the pure spectra of the molecule present in sample. The curve fitting algorithm can predict protein secondary structures under the amide I band (1,700-1,590 cm^{-1}) (i.e., as an α-helix, a β-pleated sheet, and a turn) (Machana *et al*., 2012). In our study, the corresponding protein secondary peaks were simulated and categorized into 5 components consisting of a β-sheet, an α-helix, and a turn (Fig. 2B).

Our results demonstrated that there was an increase in turn intensity (1,684 and 1,668 cm^{-1}) in HepG2 cells after being treated with alyssin (17.2 ± 0.9% and 23.7 ± 1.9%) and iberin (17.3 ± 0.3% and 23.9 ± 0.9%) compared to the control (15.7 ± 0.3% and 17.9 ± 0.4%). There was moreover no difference in α-helix intensity (1,657 cm^{-1}) between the ITC-treated groups (23.9-24.3%) and the control (23.6 ± 0.7%). The β-sheet intensities (1,643 and 1,631 cm^{-1}) were decreased in the alyssin- (18.8 ± 1.4% and 16.3 ± 1.2%) and iberin- (18.7 ± 0.5% and 16.1 ± 0.3%) treated group compared to the control (21.9 ± 0.5% and 20.9 ± 0.8%). For the sulforaphane-treated group, there were no statistically significant differences in the β-turn (15.9 ± 0.3% and 19.2 ± 0.7%), α-helix (24.2 ± 0.2%), and β-sheet peaks (21.5 ± 0.7 and 19.1 ± 0.3%) compared to the control (Fig. 2B). The β-turn and α-helix peaks were significantly shifted in the cells treated with alyssin and iberin (data not shown).

Cell viability

All the ITCs structures are presented in Fig. 3A. All ITCs are alkyl ITC with different carbon chain length on the side chain: iberin (3C); sulforaphane (4C); and alyssin (5C). HepG2 and Vero were treated with ITCs (0.1-160 μM) for 24 h. All ITCs exhibited concentration-dependent cytotoxic activity in HepG2. Alyssin caused the highest cytotoxicity with the lowest IC_{50} value (27.9 ± 0.4 μM), while iberin and sulforaphane exhibited a respective IC_{50} value of 55.2 ± 2.2

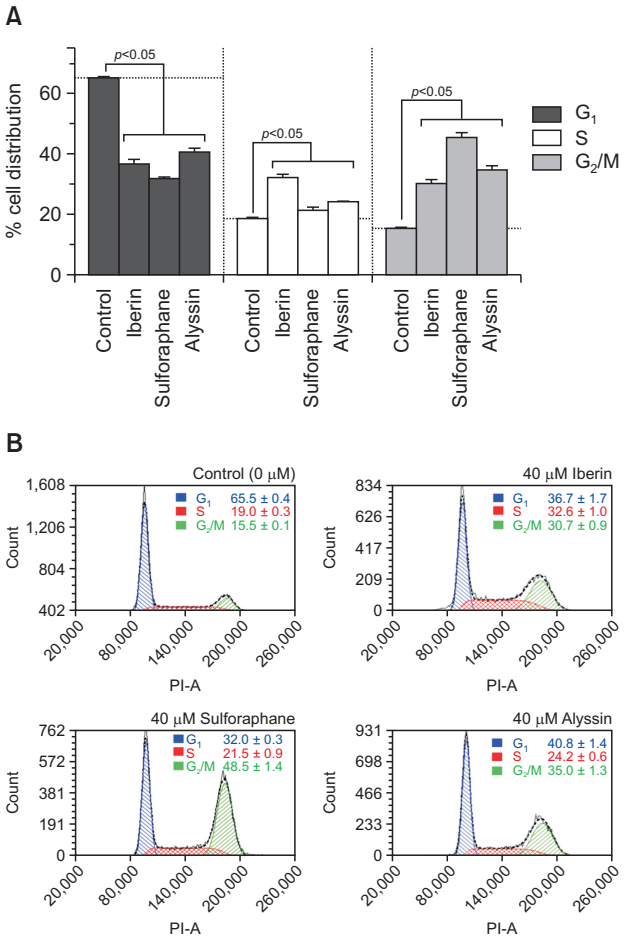

Fig. 4. Cell phase analysis of HepG2 treated with ITCs at 40 μM for 12 h; cells in G_1, S, and G_2/M phase (A), and flow cytometry histogram (B). Results expressed as mean ± SD (n=3).

and 58.9 ± 0.7 μM (Fig. 3B, 3C). The cytotoxicity profile on noncancerous cell line Vero was also determined. Alyssin induced higher cytotoxicity in the normal cell (IC_{50} of 55.9 ± 3.3 μM) than sulforaphane (99.9 ± 6.6 μM) and iberin (137.3 ± 4.6 μM), respectively (Fig. 3B, 3C). The selectivity index (SI) is the ratio indicating the cytotoxic window between normal and cancer cells, which suggests the lesser sensitive of the normal cell (Vero) to ITCs when compared to the cancer cell (HepG2) (Fig. 3B).

Mode of cell death

Mode of cell death was determined in HepG2 cells after ITC treatment at 20, 40, and 80 μM for 24 h. The Annexin V/PI staining method discriminates between living, apoptotic, and necrotic cells. Apoptotic cell death is preferable to necrotic cell death, because it causes less of an inflammatory response. All ITCs induced both HepG2 apoptotic and necrotic cell death in a dose-dependent manner (Supplementary Table 1). At 80 μM, alyssin (21.3 ± 3.6%) showed the lowest number of living cells compared to iberin (41.1 ± 0.6%), sulforaphane (54.9 ± 2.3%), and control (88.7 ± 0.9%). As for induction of cell death, alyssin (56.7 ± 5.3%) displayed higher apoptosis induction than iberin (41.9 ± 3.4%) and sulforaphane (30.9 ± 2.1%), while the control (untreated) displayed 10.7 ± 1.1% apoptotic cell death. The rank of necrosis induction was alyssin (22.0 ± 1.9%) >iberin (17.0 ± 1.7%) >sulforaphane (14.3 ± 3.6%) >control (0.6 ± 0.3%) (Fig. 3D).

Cell phase arrest

HepG2 cells were incubated with ITCs for 12 h at 10, 20, and 40 μM to observe cell-phase accumulation (Supplementary Table 1). The ITCs caused a similar pattern of cell-phase accumulation, including the reduction of G_1 phase and an increase in the G_2/M phase compared to the control. S phase arrest was also triggered when the concentration of ITCs reached 40 μM (Fig. 4A, 4B).

DNA binding

The NBP assay is used to determine *in vitro* DNA alkylating activity. NBP imitates the nucleophilic site of the pyridine ring nitrogen responsible for the electrophilic interaction with alkylating agents. Our results showed that no interaction between ITCs and NBP occurred, indicating that there was no alkylating interaction (Fig. 5A). Circular dichroism (CD) was then applied to determine the possible interaction between ITCs and the calf-thymus DNA, representing a cancer DNA model. The differences in the CD chromatogram revealed a DNA secondary structural alteration, suggesting an interaction with the treated compound. No interaction was observed between ITCs and the calf-thymus DNA when compared to cisplatin (Fig. 5B), a DNA-binding anticancer agent. The CD result agrees with the NBP result confirming that there was no interaction between DNA and ITCs under the studied conditions.

Intracellular ROS level

The intracellular ROS level was presented as a %fluorescent intensity to total cell population. The HepG2 cells were treated with ITCs at difference concentrations (10, 20, and 40 μM) for 12 h. All ITCs induced intracellular ROS levels in a concentration-dependent manner (Supplementary Table 1). At 40 μM, alyssin (36.1 ± 3.6%) induced the highest intracellular ROS level compared to iberin (25.4 ± 2.2%) and sulforaphane

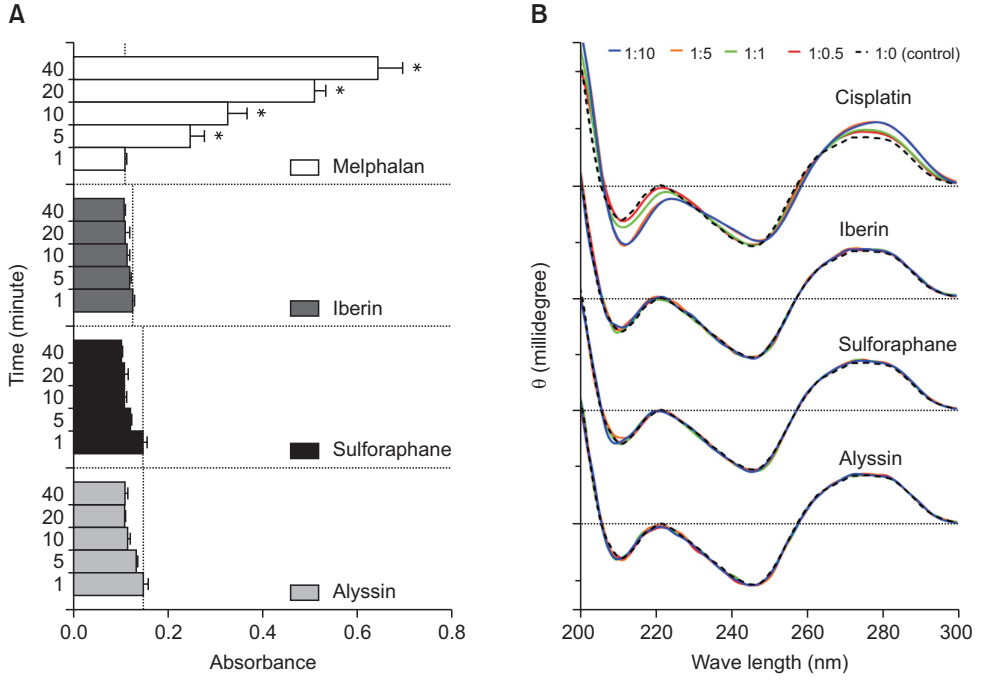

Fig. 5. ITCs-DNA interactions. Alkylating activity of ITCs compared with melphalan (positive control) according to NBP assay (A). CD spectra of calf-thymus DNA at constant concentration (50 μM) after incubated with ITCs or cisplatin (positive control) at various concentrations (25-500 μM) (B). In NBP assay, results displayed as mean ± SD (n=3) and asterisk (*) indicates statistically significant increases (p<0.05) compared to absorbance at 1 min in each treatment group.

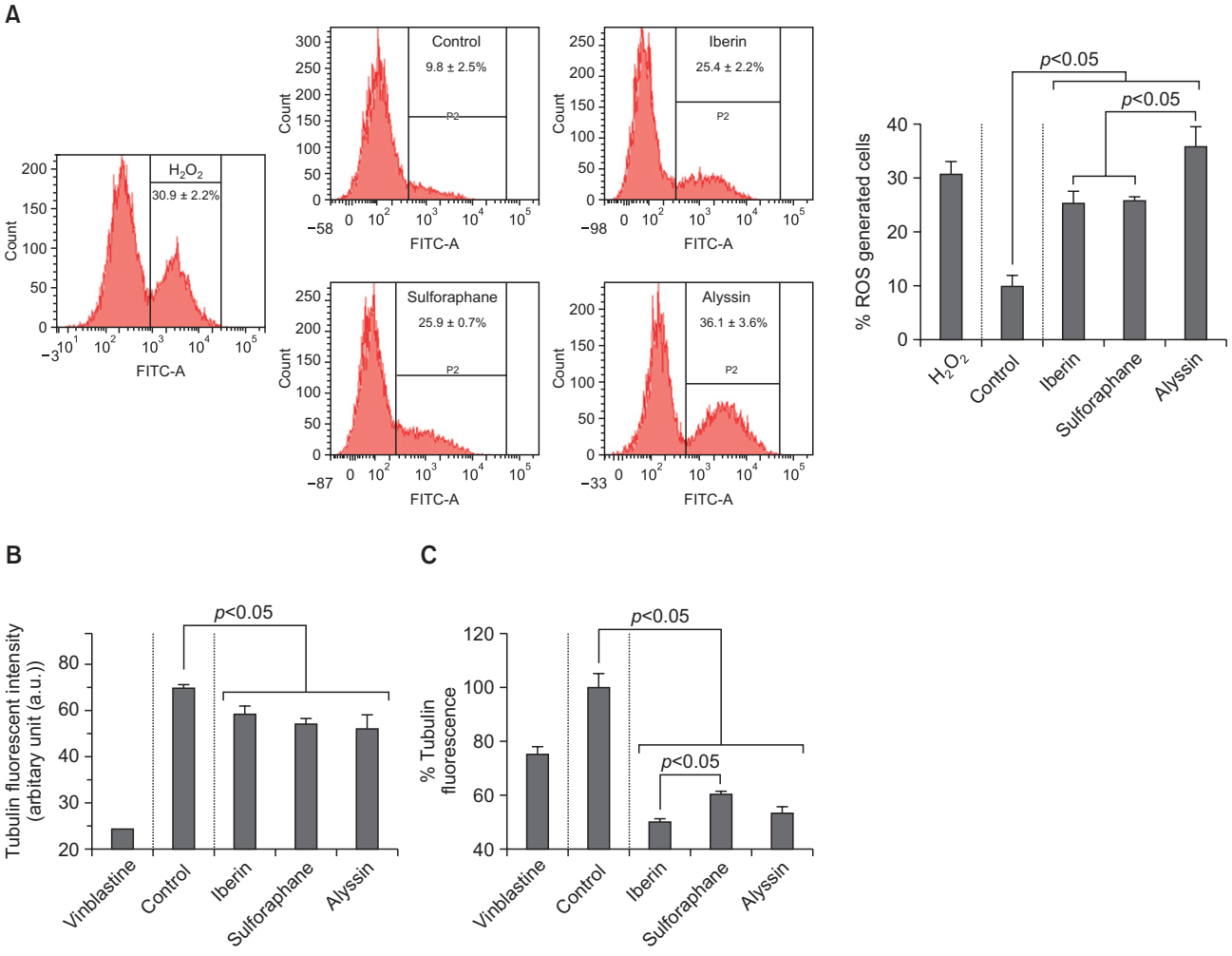

Fig. 6. Effect of ITCs on intracellular ROS level and tubulin polymerization. Flow cytometry histogram and percentage of ROS generated cells of HepG2 after ITC treatment (40 μM for 12 h) (A). *In vitro* tubulin polymerization activity of ITCs (40 μM) on purified tubulin at 60 min (B). Cell-based tubulin polymerization activity of ITCs (40 μM for 12 h) on HepG2. Values expressed as mean ± SD (n=3).

(25.9 ± 0.7%), while the control (untreated) exhibited 9.8 ± 2.5% of the intracellular ROS level. H_2O_2 (40 μM) which was used as a positive control, induced the intracellular ROS generation (30.9 ± 2.2%) (Fig. 6A).

Tubulin polymerization

The effect of ITCs on tubulin polymerization was demonstrated by *in vitro* tubulin polymerization assay. The microtubule elongation—assembling of tubulin subunits—was tracked kinetically using fluorescent spectroscopy. Tubulin polymerizations were suppressed by all ITCs (40 μM)—iberin (64.0 ± 2.7 a.u.), sulforaphane (60.6 ± 2.3 a.u.), and alyssin (59.6 ± 4.3 a.u.)—compared to the control (71.5 ± 1.9 a.u.). Vinblastine (microtubule-depolymerizing agent) was used as a positive control and suppressed tubulin polymerization (26.9 a.u.) (Fig. 6B). These results agree with a cell-based assay of tubulin polymerization study on HepG2 cells. Tubulin polymerization of the control (untreated) was normalized to 100.0 ± 5.1%. All ITCs at 12 h decreased tubulin polymerization in a dose-dependent manner (Supplementary Table 1). The tubulin polymerization (40 μM, 12 h) by alyssin (53.2 ±2.4%) was not statistically different from iberin (49.7 ± 1.6%) but was lower than sulforaphane (60.1 ± 1.4%) and vinblastine (75.1 ± 2.9%) (Fig. 6C).

DNA and microtubule staining

After treatment with ITCs (40 μM) for 12 h, HepG2 cells were stained by DAPI (magenta) and anti-tubulin antibody (green) to examine any morphological alteration of the DNA and microtubules. Nuclei DNA in the control group emitted a constant fluorescence, reflecting unharmed chromatin (i.e., not having either damaged DNA or apoptosis). By contrast, ITC-treated HepG2 cells displayed smaller and brighter chromosomes with heterogeneous staining that indicated chromatin condensation in the early stages of the apoptotic process. The anti-tubulin antibody staining in the control group exhibited continuous staining throughout the cytoplasm. These results illustrate the fine microtubule-related components (i.e., the cytoskeleton inside cells). After incubating with ITCs, microtubule aggregations were detected. Fading of microtubules was also observed in alyssin-treated HepG2 cells, indicating the process of microtubule degradation (Fig. 7). The results delineated the role of ITCs in apoptosis induc-

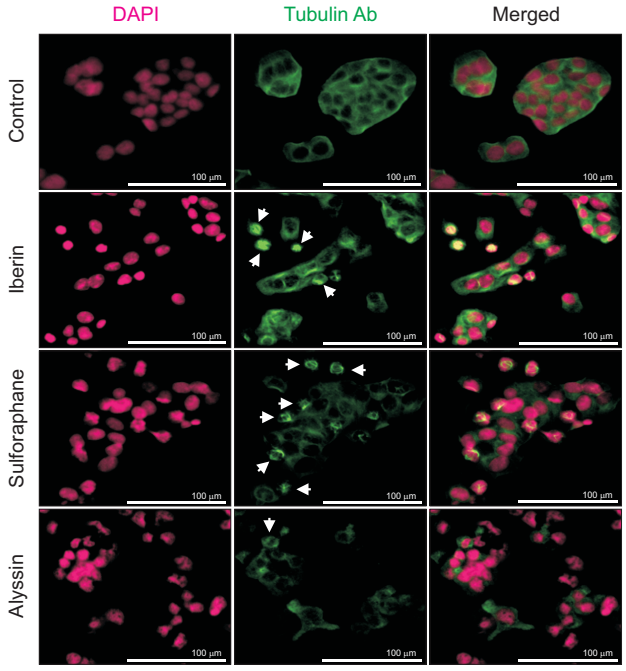

Fig. 7. DNA and microtubule morphology in HepG2 after ITC treatment at 40 μM for 12 h. DNA (magenta) in ITC-treated HepG2 condensed, suggesting occurrence of early-state apoptosis. Microtubule/tubulin (green), indicated by arrow, demonstrates microtubule aggregation. In alyssin-treated HepG2 cells, degradation process noted as microtubule/tubulin almost dissipated.

tion as well as microtubule/tubulin depolymerization.

DISCUSSION

There was no direct interaction between ITCs and DNA under our studied condition, which agrees with a report on human lung carcinoma cell A549, using radio-labelled sulforaphane and phenethyl isothiocyanate (Mi *et al*., 2011). By contrast, in an *in vitro* study on interaction between sulforaphane and DNA, the concentration required for a sulforaphane-DNA interaction was >25 mM (Abassi Joozdani *et al*., 2015) so it was not physiologically achievable. Indirect interactions between ITCs and DNA have been reportedly triggered by (1) generating intracellular ROS that cause further DNA damage (Sestili and Fimognari, 2015) and (2) inhibiting histone deacetylase (HDAC), resulting in unwrapping chromatin and making DNA prone to the repair and damage process (Rajendran *et al*., 2013).

ITCs could act either as both pro-oxidant (increasing intracellular ROS; >10 μM) or anti-oxidant (decreasing intracellular ROS; <10 μM) depending on concentration based on cell assays (Sestili and Fimognari, 2015). The current study used ITCs at a high concentration (>10 μM) and all ITCs were found to act as pro-oxidants by producing intracellular ROS. There were two major underlying mechanisms reported on how ITCs generate ROS inside the cell: (1) decreasing intracellular glutathione (Ferreira de Oliveira *et al*., 2014), and (2) disrupting electron transport in mitochondria (Xiao *et al*., 2010; Sestili and Fimognari, 2015). Excess ROSs can trigger apoptotic cell death through both the death receptor (extrinsic) pathway and the mitochondrial (intrinsic) pathway (Galadari *et al*., 2017). ITCs are hypothesized to induce cancer cell death mainly through the mitochondrial pathway due to their activity in enhancing excess ROS production in mitochondria. ITCs—like sulforaphane, phenethyl isothiocyanate, and benzyl isothiocyanate—are reported to disrupt the mitochondrial membrane potential, leading to the release of cytochrome-c triggering apoptotic cell death (Xiao *et al*., 2008). Other ITCs studies demonstrated ITC induction of apoptosis through the death receptor pathway involving induction of TRAIL receptor expression in human osteosarcoma cells (Saos2 and MG63) (Matsui *et al*., 2006) as well as increasing Fas receptor and ligand expression in the leukemia cell HL-60 (Shang *et al*., 2017). The relevant mechanisms leading to expression of these proteins at the molecular level have yet to be determined. In addition, high and prolonged intracellular ROS is able to oxidize randomly cellular components, abolishing its structure and function, resulting in necrotic cell death (Al-Qenaei *et al*., 2014).

Polymerization of tubulin forms a microtubule, which is a tubular-shaped protein polymer. The microtubule plays a pivotal role in cellular function, especially in the cell division process. Our results indicate that tubulin polymerization was directly suppressed *in vitro* by all of the ITCs. The result agrees with cell-based assays; as tubulin depolymerization was observed. Some ITCs—such as, erucin, benzyl isothiocyanate, allyl isothiocyanate, and sulforaphane—are reported to interact covalently with tubulin (Mi *et al*., 2011; Azarenko *et al*., 2014). Interfering tubulin by binding agents disables microtubule functions. The microtubule then loses the ability to attach to the centromere and properly orients the sister chromatid at the equatorial plate. The cells are then unable to progress through the metaphase and arrest in mitosis (G_2/M phase). The event triggers a cascade of activations which sequentially lead to apoptotic cell death (Clarke and Allan, 2009). In our experiment, we found the G_2/M phase arrest in all ITC treated cells as well as cell death were mainly by apoptosis. Treatment of sulforaphane in the human bladder cancer cells 5637 led to cell-cycle arrest in the G_2/M phase (Park *et al*., 2014), while the other ITCs were found to reduce the expression of anti-apoptotic proteins (Zhou *et al*., 2013; Gupta *et al*., 2014). Both consequently led to cell death by apoptosis. These results help to clarify the role of ITCs in induction of apoptosis through specific cell phase (G_2/M) arrest by disrupting tubulin polymerization. In contrast, ROS-mediated cell death was not cell-phase specific since the excessive ROS oxidized cell organelles in a non-specific pattern and thus randomly shut down the cells at non-specific phases (Verbon *et al*., 2012).

Our result indicated the lesser ITCs cytotoxicity in the normal cell compared with the cancer cell (SI ~1.7-2.5). Our result is agreement with the previous reports that cancerous cells were more sensitive to ITC than normal cells (Clarke *et al*., 2011; Kallifatidis *et al*., 2011). Sulforaphane (50 μM) previously showed no cytotoxicity in primary human hepatocyte at 48 h (Gross-Steinmeyer *et al*., 2010). Both sulforaphane and iberin displayed no toxicity in primary rat hepatocyte at 40 μM after 24 h treament (La Marca *et al*., 2012). Cancer expresses several proteins (i.e., HDAC and tubulin) for supporting their growth, which were the targets of ITCs to exert their anticancer activity (Clarke *et al*., 2011). The over-expressions of these proteins, therefore, possibly are the determinants that influence the cytotoxicity of cancerous over normal cells. For instance, tubulin is an important protein for cell division, ITCs

could arrest cell growth and induce apoptosis in fast-dividing, pre-neoplastic, and cancerous cells than their normal counterparts (Mi *et al*., 2008).

The SR-FTIR in the current study yielded a perspective on the alteration of global biochemical components of HepG2 cells after treatment with ITCs. The IR spectra in the lipid regions are increased after ITC treatment. The apoptotic process positively relates to the lipid content in the prostate cancer cell line PC3 (Gasper *et al*., 2011) and the lymphoma cell line U937 (Zelig *et al*., 2009). These studies proposed that membrane-transformation mechanisms like blebbing are possibly responsible for the increase in lipids. Our results showed that the IR spectra of the nucleic acid region were increased in tandem with apoptotic cell death, which agrees with a previous study where a leukemic T cell line was treated with etoposide to induce apoptosis (Lamberti *et al*., 2010). These results differed from prior studies showing that the IR spectra at the nucleic acid region were reduced upon apoptosis because of degradation of DNA by DNase and condensation of DNA that makes its structure opaque to infrared light (Zelig *et al*., 2009). We hypothesize that the partial increase of S phase cell, in concert with necrotic cell death, after ITCs incubation could contribute to the observed result. Chromatin relaxation during DNA synthesis in S phase as well as DNA deconvolution—due to its conformational and functional loss during necrosis—decreases chromatin opacity (Mourant *et al*., 2003). The reduction of chromosome opacity makes nucleic acid more visible to infrared light enhancing the IR spectra at the nucleic acid region (Zelig *et al*., 2009).

In the protein region, the amide I band is particularly sensitive to the secondary protein structure because of the different hydrogen-bonding environments for an α-helix, a β-sheet, and a turn conformation (Miller *et al*., 2013). Our results align with the reports indicating a decrease in a β-sheet which possibly converted from a turn, unordered, or α-helix (Lamberti *et al*., 2010; Gao *et al*., 2015); although this mechanism contradicts other reports (Zelig *et al*., 2009; Machana *et al*., 2012). The secondary contents appear to vary depending on cell types and cell death-inducing agents (Gasper *et al*., 2009; Di Giambattista *et al*., 2011). The alteration in apoptotic-related proteins has also been posited to affect secondary structures (Machana *et al*., 2012). The covalent binding of ITCs to tubulin causes a conformational change in tubulin, leading to tubulin aggregation and proteasome-dependent degradation; as has been observed in the cervical cancer cell HeLa (Mi *et al*., 2009). Microtubule/tubulin aggregation and degradation was also detected in our experiment, which could have led to the total protein content reduction as indicated by our IR integral area histogram.

ITC structure contains electrophilic character (ITC moiety) that enables the compounds to react with some nucleophilic agents containing i.e. amine, hydroxyl, thiol, and carboxylic functional group. ITCs are known to be hydrolyzed very slowly in purified water (Luang-In and Rossiter, 2015). The reaction of ITCs with amine and hydroxyl is irreversible and associated with the loss of pharmacological activity. In contrast, reaction of ITCs with thiol is about 1,000 times faster and reversible (Kaschula and Hunter, 2016). Therefore, conjugation between ITCs and GSH—which is the most abundant thiol-containing molecule within the cell—plays an important part as an intracellular ITC pool. On the other side, the GSH conjugation is considered as a transport form of the parent ITC before active (binding to targets) or inactive (being metabolized) (Shibata *et al*., 2011).

The influence of structural variation at ITC side chain—including the oxidation state of sulfur atom, number of double bond, and number of aromatic ring—on anticancer activity were investigated in our previous study (Pocasap *et al*., 2018). In the current study, a correlation analysis of the experimental parameters was performed to investigate the impact of structural attributions on the observed results (Table 1). The alkyl chain lengths between the isothiocyanate and sulfinyl moieties were different among iberin (C3), sulforaphane (C4), and alyssin (C5). The correlation analysis indicated that the anticancer activity parameters were increased as well as that of intracellular ROS, according to the slope analysis. Nevertheless the R^2 obtained from the linear regression model in most experiments suggests that there is insufficient correlation. We hypothesized that the limited structural differences in carbon length (C3-C5) were inadequate to draw any conclusion. Bond length from C3 to C5 may not yield enough structural space to alter the interaction between ITC and its targets. Clear structural-activity relationships were not discernible after inhibition of the oncogenic transcriptor (STAT3) and Nocth signaling in a prostate cancer cell line, due to the limitation of having only 3 ITCs with a range in alkyl length of C3-C5 (Hahm and Singh, 2010; Hahm *et al*., 2012). The respective impacts of ITC alkyl chain length, ranging from C2-C8, were previously reported to be positively correlated with the NQO enzyme in murine hepatoma cell Hepa1c1c7 (Hou *et al*., 2000) and HDAC inhi-

Table 1. Correlation between anticancer activity and ITC alkyl chain length

Activity	Alkyl chain length		
	Relation	Equation	R^2
Experimental parameter			
ROS generation	Increase	y=5.320x+7.830	0.778
In vitro tubulin depolymerization	Increase	y=2.200x+29.83	0.918
Cell-based tubulin depolymerization	Decrease	y=–1.775x+52.77	0.111
Cell cycle : G_2/M phase	Increase	y=2.165x+28.51	0.078
Cell cycle : S phase	Decrease	y=–4.205x+42.91	0.532
Necrosis	Increase	y=2.515x+7.697	0.414
Apoptosis	Increase	y=7.370x+13.68	0.324
Cell cytotoxicity	Increase	y=13.69x–2.080	0.651

bition in colon cancer cells HCT116 (Rajendran *et al*., 2013). These results were in agreement with the previous study that the inhibition of tumorigenesis in rat was enhanced when the alkyl chain of ITC increased from C1 to C6 (Wu *et al*., 2009). Therefore, using more than three ITCs with structural differences in the alkyl chain length more than three carbons might provide more conclusive evidence. Increasing chain length was supposed to enhance the ITC activity by (1) increasing hydrophobic interaction at the binding interface (producing favorable enthalpy) (Rajendran *et al*., 2013), and (2) diminishing the reaction rate of ITC toward GSH (Jiao *et al*., 1994). Due to GSH acts as a major intracellular ITC pool, the decreasing rate of ITC-GSH interaction lead to an increasing free-form of ITC for binding with other molecular targets and enhanced ITC activity. In our study, despite the inconclusive correlation between side-chain length and anticancer activity, our results demonstrated that alyssin was the most potent vis-à-vis cell death induction in HepG2 cells; possibly by induction of intracellular ROS as opposed to tubulin depolymerization. To wit, ROS have more impact on alyssin-induced cell death than tubulin depolymerization.

This is the first report on the chemotherapeutic activity of iberin and alyssin through induction of cancer cell death by increasing intracellular ROS and tubulin depolymerization. These compounds displayed chemotherapeutic activity in comparable with sulforaphane that is used as a nutraceutical (Prakash and Gupta, 2012), and therefore our work imply the potential of both alyssin and iberin as adjunctive agents. Iberin, sulforaphane, and alyssin have been identified in several *Brassica* plants. Alyssin was also found in *Alyssum* (*Brassicaceae*) plants, in the form of glucosinolates. *Alyssum* contains a high amount of total glucosinolates ranging from 9.9 to 135.4 μmol/g dried material (Blažević *et al*., 2016) that could be considered as an alternative source of both total ITCs and alyssin. Our study supported the use of ITCs—especially alyssin—because of its higher activity in comparison with the well-studied sulforaphane.

In conclusion, the current study determined the anticancer activity—defined by induction of cancer cell death—of ITCs, including iberin, sulforaphane, and alyssin in HepG2 cells. The ITCs (iberin, sulforaphane, and alyssin) interacted with tubulin, suppressing tubulin polymerization, and increased intracellular ROS level as a pro-oxidant. These effects led to cell-phase arrest and cancer cell death by both apoptosis and necrosis. Although the correlation between alkyl side chain length and anticancer activity was not conclusive, the highest anticancer activity was achieved by alyssin. Our result demonstrated the efficacy of alyssin and iberin on par with the neutraceutic sulforaphane and supports their use as health-benefit agents. The understanding of relevant mechanisms on how these ITCs exerted anticancer activity could also lead to more effective chemotherapeutic treatment and a strategy for supporting the use of these ITCs in health promotion.

CONFLICT OF INTEREST

The authors have no conflict of interest to declare.

ACKNOWLEDGMENTS

We thank (a) the Thailand Research Fund through the Royal Golden Jubilee Ph.D. Program (Grant No. PHD/0120/2557) for financial support to PP and NW; (b) Khon Kaen University for a grant support (2559-KKU-SLRI-01-08); (c) Research Instrument Center, Khon Kaen University, for the service support of flow cytometry; and, (d) Mr. Bryan Roderick Hamman for assistance with the English-language presentation.

REFERENCES

Abassi Joozdani, F., Yari, F., Abassi Joozdani, P. and Nafisi, S. (2015) Interaction of sulforaphane with DNA and RNA. *PLoS ONE* **10**, e0127541.

Agarwal, S., Jangir, D. K. and Mehrotra, R. (2013) Spectroscopic studies of the effects of anticancer drug mitoxantrone interaction with calf-thymus DNA. *J. Photochem. Photobiol. B Biol.* **120**, 177-182.

Al-Qenaei, A., Yiakouvaki, A., Reelfs, O., Santambrogio, P., Levi, S., Hall, N. D., Tyrrell, R. M. and Pourzand, C. (2014) Role of intracellular labile iron, ferritin, and antioxidant defence in resistance of chronically adapted Jurkat T cells to hydrogen peroxide. *Free Radic. Biol. Med.* **68**, 87-100.

Angelino, D. and Jeffery, E. (2014) Glucosinolate hydrolysis and bioavailability of resulting isothiocyanates: focus on glucoraphanin. *J. Funct. Foods* **7**, 67-76.

Azarenko, O., Jordan, M. A. and Wilson, L. (2014) Erucin, the major isothiocyanate in arugula (Eruca sativa), inhibits proliferation of MCF7 tumor cells by suppressing microtubule dynamics. *PLoS ONE* **9**, e100599.

Baker, M. J., Trevisan, J., Bassan, P., Bhargava, R., Butler, H. J., Dorling, K. M., Fielden, P. R., Fogarty, S. W., Fullwood, N. J., Heys, K. A., Hughes, C., Lasch, P., Martin-Hirsch, P. L., Obinaju, B., Sockalingum, G. D., Sulé-Suso, J., Strong, R. J., Walsh, M. J., Wood, B. R., Gardner, P. and Martin, F. L. (2014) Using Fourier transform IR spectroscopy to analyze biological materials. *Nat. Protoc.* **9**, 1771-1791.

Blažević, I., Montaut, S., Burčul, F. and Rollin, P. (2016) Glucosinolates: novel sources and biological potential. In Glucosinolates (J. M. Mérillon and K. G. Ramawat Eds.), pp. 1-58. Springer International Publishing, Cham.

Clarke, J. D., Hsu, A., Yu, Z., Dashwood, R. H. and Ho, E. (2011) Differential effects of sulforaphane on histone deacetylases, cell cycle arrest and apoptosis in normal prostate cells versus hyperplastic and cancerous prostate cells. *Mol. Nutr. Food Res.* **55**, 999-1009.

Clarke, P. R. and Allan, L. A. (2009) Cell-cycle control in the face of damage – a matter of life or death. *Trends Cell Biol.* **19**, 89-98.

Di Giambattista, L., Pozzi, D., Grimaldi, P., Gaudenzi, S., Morrone, S. and Congiu Castellano, A. (2011) New marker of tumor cell death revealed by ATR-FTIR spectroscopy. *Anal. Biol. Chem.* **399**, 2771-2778.

Ernst, I. M. A., Palani, K., Esatbeyoglu, T., Schwarz, K. and Rimbach, G. (2013) Synthesis and Nrf2-inducing activity of the isothiocyanates iberverin, iberin and cheirolin. *Pharmacol. Res.* **70**, 155-162.

Ferreira de Oliveira, J. M. P., Costa, M., Pedrosa, T., Pinto, P., Remédios, C., Oliveira, H., Pimentel, F., Almeida, L. and Santos, C. (2014) Sulforaphane induces oxidative stress and death by p53-independent mechanism: implication of impaired glutathione recycling. *PLoS ONE* **9**, e92980.

Galadari, S., Rahman, A., Pallichankandy, S. and Thayyullathil, F. (2017) Reactive oxygen species and cancer paradox: To promote or to suppress? *Free Radic. Biol. Med.* **104**, 144-164.

Gao, Y., Huo, X., Dong, L. I. U., Sun, X., Sai, H. E., Wei, G., Xu, Y., Zhang, Y. and Wu, J. (2015) Fourier transform infrared microspectroscopy monitoring of 5-fluorouracil-induced apoptosis in SW620 colon cancer cells. *Mol. Med. Rep.* **11**, 2585-2591.

Gasper, R., Dewelle, J., Kiss, R., Mijatovic, T. and Goormaghtigh, E. (2009) IR spectroscopy as a new tool for evidencing antitumor drug signatures. *Biochim. Biophys. Acta* **1788**, 1263-1270.

Gasper, R., Vandenbussche, G. and Goormaghtigh, E. (2011) Ouabain-induced modifications of prostate cancer cell lipidome investigated with mass spectrometry and FTIR spectroscopy. *Biochem.*

Biophys. Acta **1808**, 597-605.
Gross-Steinmeyer, K., Stapleton, P. L., Tracy, J. H., Bammler, T. K., Strom, S. C. and Eaton, D. L. (2010) Sulforaphane- and phenethyl isothiocyanate-induced inhibition of aflatoxin B1-mediated genotoxicity in human hepatocytes: role of GSTM1 genotype and CYP3A4 gene expression. *Toxicol. Sci.* **116**, 422-432.
Gupta, P., Wright, S. E., Kim, S. H. and Srivastava, S. K. (2014) Phenethyl isothiocyanate: a comprehensive review of anti-cancer mechanisms. *Biochem. Biophys. Acta* **1846**, 405-424.
Hahm, E. R., Chandra-Kuntal, K., Desai, D., Amin, S. and Singh, S. V. (2012) Notch activation is dispensable for D, L-sulforaphane-mediated inhibition of human prostate cancer cell migration. *PLoS ONE* **7**, e44957.
Hahm, E. R. and Singh, S. V. (2010) Sulforaphane inhibits constitutive and interleukin-6-induced activation of signal transducer and activator of transcription 3 in prostate cancer cells. *Cancer Prev. Res. (Phila.)* **3**, 484-494.
Hou, D. X., Fukuda, M., Fujii, M. and Fuke, Y. (2000) Induction of NADPH:quinone oxidoreductase in murine hepatoma cells by methylsulfinyl isothiocyanates: methyl chain length-activity study. *Int. J. Mol. Med.* **6**, 441-444.
Jadhav, U., Ezhilarasan, R., Vaughn, S. F., Berhow, M. A. and Mohanam, S. (2007) Iberin induces cell cycle arrest and apoptosis in human neuroblastoma cells. *Int. J. Mol. Med.* **19**, 353-361.
Jakubikova, J., Bao, Y., Bodo, J. and Sedlak, J. (2006) Isothiocyanate iberin modulates phase II enzymes, posttranslational modification of histones and inhibits growth of Caco-2 cells by inducing apoptosis. *Neoplasma* **53**, 463-470.
Jiao, D., Eklind, K. I., Choi, C. I., Desai, D. H., Amin, S. G. and Chung, F. L. (1994) Structure-activity relationships of isothiocyanates as mechanism-based inhibitors of 4-(methylnitrosamino)-1-(3-pyridyl)-1-butanone-induced lung tumorigenesis in A/J mice. *Cancer Res.* **54**, 4327-4333.
Junhom, C., Weerapreeyakul, N., Tanthanuch, W. and Thumanu, K. (2016) FTIR microspectroscopy defines early drug resistant human hepatocellular carcinoma (HepG2) cells. *Exp. Cell Res.* **340**, 71-80.
Kallifatidis, G., Labsch, S., Rausch, V., Mattern, J., Gladkich, J., Moldenhauer, G., Büchler, M. W., Salnikov, A. V. and Herr, I. (2011) Sulforaphane increases drug-mediated cytotoxicity toward cancer stem-like cells of pancreas and prostate. *Mol. Ther.* **19**, 188-195.
Kaschula, C. H. and Hunter, R. (2016) Chapter 1 - Synthesis and structure–activity relations in allylsulfide and isothiocyanate compounds from garlic and broccoli against *in vitro* cancer cell growth. In Studies in Natural Products Chemistry (R. Atta-ur Ed.), pp. 1-43. Elsevier.
La Marca, M., Beffy, P., Della Croce, C., Gervasi, P. G., Iori, R., Puccinelli, E. and Longo, V. (2012) Structural influence of isothiocyanates on expression of cytochrome P450, phase II enzymes, and activation of Nrf2 in primary rat hepatocytes. *Food Chem. Toxicol.* **50**, 2822-2830.
Lamberti, A., Sanges, C. and Arcari, P. (2010) FT-IR spectromicroscopy of mammalian cell cultures during necrosis and apoptosis induced by drugs. *Spectroscopy* **24**, 535-546.
Luang-In, V. and Rossiter, J. T. (2015) Stability studies of isothiocyanates and nitriles in aqueous media. *Songklanakarin J. Sci. Technol.* **37**, 625-630.
Machana, S., Weerapreeyakul, N., Barusrux, S., Thumanu, K. and Tanthanuch, W. (2012) FTIR microspectroscopy discriminates anticancer action on human leukemic cells by extracts of *Pinus kesiya; Cratoxylum formosum* ssp. *pruniflorum* and melphalan. *Talanta* **93**, 371-382.
Matsui, T. A., Sowa, Y., Yoshida, T., Murata, H., Horinaka, M., Wakada, M., Nakanishi, R., Sakabe, T., Kubo, T. and Sakai, T. (2006) Sulforaphane enhances TRAIL-induced apoptosis through the induction of DR5 expression in human osteosarcoma cells. *Carcinogenesis* **27**, 1768-1777.
Mi, L., Di Pasqua, A. J. and Chung, F. L. (2011) Proteins as binding targets of isothiocyanates in cancer prevention. *Carcinogenesis* **32**, 1405-1413.
Mi, L., Gan, N., Cheema, A., Dakshanamurthy, S., Wang, X., Yang, D. C. and Chung, F. L. (2009) Cancer preventive isothiocyanates induce selective degradation of cellular alpha- and beta-tubulins by proteasomes. *J. Biol. Chem.* **284**, 17039-17051.
Mi, L., Xiao, Z., Hood, B. L., Dakshanamurthy, S., Wang, X., Govind, S., Conrads, T. P., Veenstra, T. D. and Chung, F. L. (2008) Covalent binding to tubulin by isothiocyanates. A mechanism of cell growth arrest and apoptosis. *J. Biol. Chem.* **283**, 22136-22146.
Miller, L. M., Bourassa, M. W. and Smith, R. J. (2013) FTIR spectroscopic imaging of protein aggregation in living cells. *Biochim. Biophys. Acta* **1828**, 2339-2346.
Misiewicz, I., Skupinska, K. and Kasprzycka-Guttman, T. (2007) Differential response of human healthy lymphoblastoid and CCRF-SB leukemia cells to sulforaphane and its two analogues: 2-oxohexyl isothiocyanate and alyssin. *Pharmacol. Rep.* **59**, 80-87.
Mourant, J. R., Yamada, Y. R., Carpenter, S., Dominique, L. R. and Freyer, J. P. (2003) FTIR spectroscopy demonstrates biochemical differences in mammalian cell cultures at different growth stages. *Biophys. J.* **85**, 1938-1947.
Nonpunya, A., Sethabouppha, B., Rufini, S. and Weerapreeyakul, N. (2018) *Cratoxylum formosum* ssp. *pruniflorum* activates the TRAIL death receptor complex and inhibits topoisomerase I. *S. Afr. J. Bot.* **114**, 150-162.
Park, H. S., Han, M. H., Kim, G. Y., Moon, S. K., Kim, W. J., Hwang, H. J., Park, K. Y. and Choi, Y. H. (2014) Sulforaphane induces reactive oxygen species-mediated mitotic arrest and subsequent apoptosis in human bladder cancer 5637 cells. *Food Chem. Toxicol.* **64**, 157-165.
Pocasap, P., Weerapreeyakul, N. and Barusrux, S. (2013) Cancer preventive effect of Thai rat-tailed radish (*Raphanus sativus* L. var. *caudatus* Alef). *J. Funct Foods* **5**, 1372-1381.
Pocasap, P., Weerapreeyakul, N. and Thumanu, K. (2018) Structures of isothiocyanates attributed to reactive oxygen species generation and microtubule depolymerization in HepG2 cells. *Biomed. Pharmacother.* **101**, 698-709.
Prakash, D. and Gupta, C. (2012) Glucosinolates: the phytochemicals of nutraceutical importance. *J. Complement. Integr. Med.* **9**, Article 13.
Rajendran, P., Kidane, A. I., Yu, T.-W., Dashwood, W.-M., Bisson, W. H., Löhr, C. V., Ho, E., Williams, D. E. and Dashwood, R. H. (2013) HDAC turnover, CtIP acetylation and dysregulated DNA damage signaling in colon cancer cells treated with sulforaphane and related dietary isothiocyanates. *Epigenetics* **8**, 612-623.
Sestili, P. and Fimognari, C. (2015) Cytotoxic and antitumor activity of sulforaphane: the role of reactive oxygen species. *BioMed Res. Int.* **2015**, 9.
Shang, H. S., Shih, Y. L., Lee, C. H., Hsueh, S. C., Liu, J. Y., Liao, N. C., Chen, Y. L., Huang, Y. P., Lu, H. F. and Chung, J. G. (2017) Sulforaphane-induced apoptosis in human leukemia HL-60 cells through extrinsic and intrinsic signal pathways and altering associated genes expression assayed by cDNA microarray. *Environ. Toxicol.* **32**, 311-328.
Shibata, T., Kimura, Y., Mukai, A., Mori, H., Ito, S., Asaka, Y., Oe, S., Tanaka, H., Takahashi, T. and Uchida, K. (2011) Transthiocarbamoylation of proteins by thiolated isothiocyanates. *J. Biol. Chem.* **286**, 42150-42161.
Skupinska, K., Misiewicz-Krzeminska, I., Lubelska, K. and Kasprzycka-Guttman, T. (2009) The effect of isothiocyanates on CYP1A1 and CYP1A2 activities induced by polycyclic aromatic hydrocarbons in Mcf7 cells. *Toxicol. In Vitro* **23**, 763-771.
Tian, G., Li, Y., Cheng, L., Yuan, Q., Tang, P., Kuang, P. and Hu, J. (2016) The mechanism of sulforaphene degradation to different water contents. *Food Chem.* **194**, 1022-1027.
Traka, M. H. (2016) Health benefits of glucosinolates. *Adv. Bot. Res.* **80**, 247-279.
Veeranki, O. L., Bhattacharya, A., Tang, L., Marshall, J. R. and Zhang, Y. (2015) Cruciferous vegetables, isothiocyanates, and prevention of bladder bancer. *Curr. Pharmacol. Rep.* **1**, 272-282.
Verbon, E. H., Post, J. A. and Boonstra, J. (2012) The influence of reactive oxygen species on cell cycle progression in mammalian cells. *Gene* **511**, 1-6.
Wang, W., Wang, S., Howie, A. F., Beckett, G. J., Mithen, R. and Bao, Y. (2005) Sulforaphane, erucin, and iberin up-regulate thioredoxin reductase 1 expression in human MCF-7 cells. *J. Agric. Food*

Chem. **53**, 1417-1421.
Wu, X., Zhou, Q. H. and Xu, K. (2009) Are isothiocyanates potential anti-cancer drugs? *Acta Pharmacol. Sin.* **30**, 501-512.
Xiao, D., Powolny, A. A., Moura, M. B., Kelley, E. E., Bommareddy, A., Kim, S. H., Hahm, E. R., Normolle, D., Van Houten, B. and Singh, S. V. (2010) Phenethyl isothiocyanate inhibits oxidative phosphorylation to trigger reactive oxygen species-mediated death of human prostate cancer cells. *J. Biol. Chem.* **285**, 26558-26569.
Xiao, D., Powolny, A. A. and Singh, S. V. (2008) Benzyl isothiocyanate targets mitochondrial respiratory chain to trigger reactive oxygen species-dependent apoptosis in human breast cancer cells. *J. Biol. Chem.* **283**, 30151-30163.
Zelig, U., Kapelushnik, J., Moreh, R., Mordechai, S. and Nathan, I. (2009) Diagnosis of cell death by means of infrared spectroscopy. *Biophys. J.* **97**, 2107-2114.
Zhou, T., Li, G., Cao, B., Liu, L., Cheng, Q., Kong, H., Shan, C., Huang, X., Chen, J. and Gao, N. (2013) Downregulation of Mcl-1 through inhibition of translation contributes to benzyl isothiocyanate-induced cell cycle arrest and apoptosis in human leukemia cells. *Cell Death Dis.* **4**, e515.